Hyperfine Interactions **153:** 25–41, 2004.

An Overview of ^{166}Er, ^{169}Tm and ^{170}Yb Mössbauer Spectroscopy

J. M. CADOGAN[1] and D. H. RYAN[2]
[1]*School of Physics, The University of New South Wales, Sydney, NSW 2052, Australia*
[2]*Centre for the Physics of Materials, Department of Physics, McGill University, Rutherford Building, 3600 University Street, Montreal, PQ, Canada H3A 2T8*

Abstract. The hyperfine splittings of the nuclear energy levels in rare-earth (R) isotopes are sensitive measures of the complex interplay between magnetic exchange and electrostatic crystal-field interactions operating at the atomic level. Mössbauer spectroscopy has been used to great effect in the on-going investigation of these fundamental interactions in R compounds and in this paper we present an overview of ^{166}Er, ^{169}Tm and ^{170}Yb Mössbauer spectroscopy. In particular, we derive expressions for the nuclear energy level splittings incorporating both magnetic and electric quadrupole interactions, using second-order perturbation theory. Such expressions provide a useful means of fitting experimental spectra and also yield criteria for determining whether or not a proposed set of energy level values is physical or not. We also present a number of useful *rules of thumb* for the analysis of ^{166}Er, ^{169}Tm and ^{170}Yb Mössbauer spectra and, as such, this paper is in effect a *Resource Letter*.

Key words: rare-earths, Mössbauer spectroscopy, crystal-fields.

1. Introduction

The rare-earth (R) or lanthanide elements may be quite similar chemically but this series presents an extremely rich variety of magnetic behaviour, associated with the progressive filling of the 4f electron shell. Their magnetism is dictated by the complex interplay between magnetic exchange and crystal-field interactions and the localized nature of the 4f electron shell provides an excellent arena in which to study this interplay. Mössbauer spectroscopy has made an enormous contribution to the study of magnetism in metallic and non-metallic rare-earth compounds alike.

The R series comprises elements La (#57) to Lu (#71), inclusive, and Mössbauer transitions have been found in each R element except Ce (#58). A total of 39 isotopes show at least one Mössbauer transition and across the series 49 transitions have been observed [1]. While none of these transitions is as straightforward as ^{57}Fe or ^{119}Sn, and most are extremely difficult to utilise, several are routinely studied and in this paper we present an overview of Mössbauer spectroscopy in three amenable R isotopes, ^{166}Er, ^{169}Tm and ^{170}Yb. In the following paper [2] we will illustrate their use with examples taken from our recent work on the intermetallic compounds $ErFe_6Sn_6$, Er_3Ge_4 and $YbMn_2(Ge,Si)_2$.

Table I. Useful Mössbauer transition data

	^{166}Er	^{169}Tm	^{170}Yb
Isotopic abundance (%)	33.41	100.0	3.03
Transition energy (keV)	80.557(4)	8.401(8)	84.253(1)
Excited state spin	2^+	$\frac{3}{2}^+$	2^+
Ground state spin	0^+	$\frac{1}{2}^+$	0^+
Excited state half-life (ns)	1.87(3)	4.00(10)	1.608(17)
Internal conversion coefficient	6.93(3)	268(5)	8.05(20)
Natural linewidth (mm/s)	2.04(4)	8.1(2)	2.02(2)
Excited state magnetic moment (μ_N)	0.629(10)	0.534(10)	0.669(8)
Excited state gyromagnetic ratio (mm/s /T)	0.0369(6)	0.400(8)	0.0375(4)
Ground state magnetic moment (μ_N)	0	−0.2310(15)	0
Ground state gyromagnetic ratio (mm/s /T)	0	−0.520(3)	0
Excited state electric quadrupole moment (barns)	−1.59(15)	−1.20(7)	−2.11(11)
Ground state electric quadrupole moment (barns)	0	0	0
Energy equivalent of 1 mm/s in joules ($\times 10^{-27}$)	43.052(1)	4.490(6)	45.0275(8)
Energy equivalent of 1 mm/s in MHz	64.973(1)	6.776(6)	67.954(8)
Energy equivalent of 1 mm/s in mK	3.1182(1)	0.3252(6)	3.2613(8)
Free-ion hyperfine field (T) [3, 4]	770.5 ± 10.5	668.8	416.6 ± 1.2
Source half-life	26 h	9.4 d	130 d

2. Mössbauer transitions

In Table I we give a summary of the principal Mössbauer transitions in ^{166}Er, ^{169}Tm and ^{170}Yb, together with a compendium of various constants relating to the nuclear energy levels involved in these transitions. Most of these data have been taken from [1].

There are three principal classes of hyperfine interaction which couple the nuclear spin system to the atomic electron system [3–8]:

- electric monopole (the *isomer shift*),
- magnetic dipole (the *hyperfine field*), and
- electric quadrupole (the *quadrupole splitting*).

In this paper we shall concentrate on the magnetic dipole and electric quadrupole interactions and so all mathematical expressions and simulated spectra given throughout this paper assume a zero isomer shift. Furthermore, in those cases where the hyperfine Hamiltonian contains off-diagonal terms the resultant eigenvectors will be admixtures of the basis states defined by the nuclear spin I and its projection m or I_z. For the purposes of clarity we shall label admixed states using

the original, 'pure' state. As an example, the final energy eigenvector resulting from the effect of the quadrupole asymmetry parameter η on, e.g., the $|m = +2\rangle$ state in ^{166}Er will be labelled as $|m = +2\rangle$ in diagrams although the state is in fact an admixture of the $|m = +2\rangle$ and $|m = 0\rangle$ states, since the relevant off-diagonal quadrupole spin operator contains the lowering operation I_-^2.

Finally, we note that the relative intensities of the six lines in a ^{169}Tm Mössbauer spectrum, arising from the $\frac{3}{2} \leftrightarrow \frac{1}{2}$ transition are 3 : 2 : 1 : 1 : 2 : 3 for a powder average whereas for the $2 \leftrightarrow 0$ transition in ^{166}Er and ^{170}Yb Mössbauer spectra the relative intensities of the five lines are 1 : 1 : 1 : 1 : 1.

3. Electronic properties

The magnetic and chemical behaviour of R elements in metallic or non-metallic compounds is generally characteristic of the tripositive R^{3+} ion and in Table II we give a summary of the electronic properties of the R^{3+} ions. At this point we can make a few important comments concerning the valence behaviour of the R elements:

- most R ions are tripositive in metallic and non-metallic compounds;
- La^{3+} and Lu^{3+} are 'non-magnetic' (in the sense of not carrying a magnetic moment) since their 4f shells are completely empty or full, respectively;
- Yb^{3+} is 'magnetic' but Yb commonly forms Yb^{2+} which has a full 4f shell and is 'non-magnetic'. The difference between the ^{170}Yb Mössbauer spectra of these two valence states can be striking [2];
- in many compounds Yb has a valence intermediate between 3+ and 2+;
- Ce^{3+} is 'magnetic' but Ce commonly forms Ce^{4+} which has an empty 4f shell and is 'non-magnetic';

Table II. Electronic properties of Er^{3+}, Tm^{3+} and Yb^{3+}

	Er^{3+}	Tm^{3+}	Yb^{3+}
Number of 4f electrons	11	12	13
Spectroscopic notation of ground manifold	$^4I_{15/2}$	$^3H_6$	$^2F_{7/2}$
Spin angular momentum S	1.5	1	0.5
Orbital angular momentum L	6	5	3
Total angular momentum J	7.5	6	3.5
Landé g-factor g_J	$\frac{6}{5}$	$\frac{7}{6}$	$\frac{8}{7}$
Maximum R^{3+} magnetic moment (μ_B) ($= g_J\|\langle J_z\rangle\|_{max} = g_J J$)	9.0	7.0	4.0
4f quadrupole term $\langle 3J_z^2 - J(J+1)\rangle$ (max)	105	66	21
de Gennes factor $(g_J - 1)^2 J(J+1)$	2.5500	1.1667	0.3214

- in many compounds both Ce and Yb exhibit heavy-fermion behaviour;
- Gd^{3+} and Eu^{2+} are *S-state* ions and have no 4f contributions to the electric field gradient (EFG) at the nucleus.

4. Calibration materials

Rare-earth Mössbauer spectroscopy often involves much larger velocity ranges than in ^{57}Fe and the use of a laser interferometer to calibrate high-speed drives is recommended. In addition, there are a number of compounds available which provide reliable velocity calibration.

^{166}Er. We propose that the cubic Laves phase compound $ErFe_2$ be used for the calibration of ^{166}Er spectrometers. First of all, the compound is quite easy to prepare in single-phase form and there is only one Er^{3+} site whose cubic point symmetry ensures no lattice contribution to the EFG (assuming there is no magnetoelestic distortion). The ^{166}Er hyperfine field at 1.4 K is 819.4 T. This calibration field is the average of the ^{166}Er Mössbauer measurement of 820.5(8) T by Hodges *et al*. [9] and the ^{167}Er NMR measurement of 818.4±10 T by Berthier and Devine [10]. It is implicit here that the so-called *hyperfine anomaly* which gives rise to a small difference in the hyperfine field experienced by different isotopes, is negligible. In any event, such a difference is probably within the experimental error of these field determinations. For example, in his recent book Guimarães [6] refers to "*an exceptionally high value of* -0.5%" for the hyperfine anomaly with ^{151}Eu and ^{153}Eu being measured in various Eu^{2+} salts by Baker and Williams [11].

^{169}Tm. For similar reasons as in the case of ^{166}Er, we propose that the cubic Laves phase compound $TmFe_2$ be used for the calibration of ^{169}Tm spectrometers. It is crucial in the case of ^{169}Tm that a Tm-compound be used for calibration rather than extrapolating a standard α-Fe calibration since the velocity range required for a fully-split ^{169}Tm magnetic spectrum is $\sim \pm 800$ mm/s, which compresses a fully-split α-Fe spectrum into one or two channels! The ^{169}Tm hyperfine field at 1.4 K is 698.6±5 T. This field has been determined by both NMR [12] and Mössbauer spectroscopy [13].

^{170}Yb. The velocity range employed in ^{170}Yb Mössbauer spectroscopy is smaller than either ^{166}Er or ^{169}Tm and there are a number of suitable materials available for calibration. We have used both $YbCrO_3$ and $YbFeO_3$ for calibration purposes [14].

5. Electric quadrupole interaction

The electric quadrupole interaction is an electrostatic coupling between the nuclear electric quadrupole moment (when $I > \frac{1}{2}$) and any electric field gradients (EFG) existing at the nucleus. The EFG contains contributions from the 4f electronic shell

Table III. Second-order nuclear spin operators (O^a_{nm}), quadrupole parameters (P^a_{nm}) and their proportionality relationships to the EFG tensor components (V_{ij})

O_{20}	O^c_{21}	O^s_{21}	O^c_{22}	O^s_{22}
$3I_z^2 - I^2$	$\frac{1}{2}(I_z I_x + I_x I_z)$	$\frac{1}{2}(I_z I_y + I_y I_z)$	$I_x^2 - I_y^2$	$(I_x I_y + I_y I_x)$
P_{20}	P^c_{21}	P^s_{21}	P^c_{22}	P^s_{22}
V_{zz}	$4V_{xz}$	$4V_{yz}$	$V_{xx} - V_{yy}$	$2V_{xy}$
V_{zz}	V_{xz}	V_{yz}	$V_{xx} - V_{yy}$	V_{xy}
$\sum_i \frac{(3z_i^2 - r_i^2)}{r_i^5}$	$\sum_i \frac{(3x_i z_i)}{r_i^5}$	$\sum_i \frac{(3y_i z_i)}{r_i^5}$	$\sum_i \frac{3(x_i^2 - y_i^2)}{r_i^5}$	$\sum_i \frac{(3x_i y_i)}{r_i^5}$

of the parent R^{3+} ion and the surrounding charges (including conduction electrons) in the lattice. There is also a substantial contribution from the asphericity of the valence-electron charge density as shown by Coehoorn *et al.* [15]. This is an important point as it means that the usual assumption of direct proportionality between the non-4f EFG and the second-order crystal-field summations, in particular the assumption that $V_{zz} \propto A_{20}$, using standard notation, lacks a physical basis and is in effect a useful approximation. For the purpose of the following discussion we will refer to '4f' and 'lattice' contributions to the total EFG at the nucleus but we ask the reader to bear in mind the *caveat* of Coehoorn's work.

The completely general form of the quadrupole Hamiltonian may be written in terms of nuclear spin operators

$$\mathcal{H}_Q = P_{20} O_{20} + P^c_{21} O^c_{21} + P^s_{21} O^s_{21} + P^c_{22} O^c_{22} + P^s_{22} O^s_{22}, \tag{1}$$

where the spin operators (O^a_{nm}) and the quadrupole parameters (P^a_{nm}) are listed in Table III.

The constant of proportionality between a quadrupole term P_{nm} and the corresponding EFG term V_{ij} is $eQ/[4I(2I - 1)]$. The EFG terms are the standard second-derivatives of the electrostatic potential

$$V_{ij} = \frac{\partial^2 V}{\partial x_i \partial x_j}.$$

It is conventional to treat the electric quadrupole interaction within a reference frame known as the principal axis system in which only the diagonal components of the EFG tensor $\{V_{ij}\}$ are nonzero (hence, $P^c_{21} = P^s_{21} = P^s_{22} = 0$). Conventionally, we select these axes such that

$$|V_{zz}| \geqslant |V_{yy}| \geqslant |V_{xx}| \tag{2}$$

and Laplace's equation yields the further constraint

$$V_{xx} + V_{yy} + V_{zz} = 0. \tag{3}$$

Table IV. Rotational transformations of the nuclear spin operators for a general orientation (θ, ϕ) of the quantization (z) axis

	O_{20}	O_{21}^s	O_{21}^c	O_{22}^c	O_{22}^s
$O_{20} \rightarrow$	$\frac{1}{2}(3\cos^2\theta - 1)$	$-3\sin 2\theta$	–	$\frac{3}{2}\sin^2\theta$	–
$O_{21}^c \rightarrow$	$\frac{1}{4}\sin 2\theta \cos\phi$	$\cos 2\theta \cos\phi$	$-\cos\theta \sin\phi$	$-\frac{1}{4}\sin^2\theta \cos\phi$	$\frac{1}{2}\sin\theta \sin\phi$
$O_{21}^s \rightarrow$	$\frac{1}{4}\sin^2\theta \sin\phi$	$\cos 2\theta \sin\phi$	$\cos\theta \cos\phi$	$-\frac{1}{4}\sin 2\theta \sin\phi$	$-\frac{1}{2}\sin\theta \cos\phi$
$O_{22}^c \rightarrow$	$\frac{1}{2}\sin^2\theta \cos 2\phi$	$\sin 2\theta \cos 2\phi$	$-2\sin\theta \sin 2\phi$	$\frac{1}{2}(1+\cos^2\theta)\cos 2\phi$	$-\cos\theta \sin 2\phi$
$O_{22}^s \rightarrow$	$\frac{1}{2}\sin^2\theta \sin 2\phi$	$\sin 2\theta \sin 2\phi$	$2\sin\theta \cos 2\phi$	$\frac{1}{2}(1+\cos^2\theta)\sin 2\phi$	$\cos\theta \cos 2\phi$

Often it is possible to use crystallographic point symmetry arguments to determine the principal axes. For example, a site with a mirror plane point symmetry will have one principal axis perpendicular to that plane and the other two axes within the plane. Unfortunately, one cannot identify the individual axes. The standard asymmetry parameter, within the principal axis system, is

$$\eta = \frac{V_{xx} - V_{yy}}{V_{zz}} = \frac{P_{22}^c}{P_{20}}$$

and if the R^{3+} ion is located at a site whose *point symmetry* is tetragonal, hexagonal or trigonal (rhombohedral) then $\eta = 0$. For cubic point symmetry, the lattice EFG vanishes. It is important to note here that the principal axes of the 4f and lattice contributions to the EFG need not coincide and in such a case it is necessary to rotate one of the reference frames onto the other. This can be achieved by the standard spin-operator rotational transformations, tabulated by Arif *et al.* [16] and reproduced in Table IV. A particularly useful tabulation of all 2nd, 4th and 6th-order spin-operator rotational transformations, used in describing the crystal-field acting on an R^{3+} ion, has been tabulated by Rudowicz [17].

This table is read as follows:

$$O_{20} \longrightarrow \frac{1}{2}\left(3\cos^2\theta - 1\right)O_{20} - 3\sin 2\theta\, O_{21}^c + \frac{3}{2}\sin^2\theta\, O_{22}^c, \tag{4}$$

where the arrow denotes the coordinate rotation. Thus, a simple electric quadrupole Hamiltonian such as

$$\mathcal{H}_Q = P_{20}O_{20} + P_{22}^c O_{22}^c \tag{5}$$

which is defined within its principal axis system, transforms to

$$\begin{aligned}\mathcal{H}_Q &= \left[\frac{1}{2}\left(3\cos^2\theta - 1\right)P_{20} + \frac{1}{2}\sin^2\theta\cos 2\phi\, P_{22}^c\right]O_{20} \\ &\quad + \left[-3\sin 2\theta\, P_{20} + \sin 2\theta\cos 2\phi\, P_{22}^c\right]O_{21}^c \\ &\quad + \left[-2\sin\theta\sin 2\phi\, P_{22}^c\right]O_{21}^s \\ &\quad + \left[\frac{3}{2}\sin^2\theta\, P_{20} + \frac{1}{2}\left(1+\cos^2\theta\right)P_{22}^c\right]O_{22}^c \\ &\quad + \left[-\cos\theta\sin 2\phi\, P_{22}^c\right]O_{22}^s \end{aligned} \tag{6}$$

within a new frame which is related to the old, principal, frame by the polar angles (θ, ϕ). Alternatively, we may consider this situation in terms of the two original quadrupole parameters, P_{20} and P_{22}^c which define the EFG, producing the following set of quadrupole parameters in the rotated frame:

$$\begin{aligned} P_{20}' &= \frac{1}{2}\left(3\cos^2\theta - 1\right)P_{20} + \frac{1}{2}\sin^2\theta\cos 2\phi\, P_{22}^c, \\ P_{21}^{c\prime} &= -3\sin 2\theta\, P_{20} + \sin 2\theta\cos 2\phi\, P_{22}^c, \\ P_{21}^{s\prime} &= -2\sin\theta\sin 2\phi\, P_{22}^c, \\ P_{22}^{c\prime} &= \frac{3}{2}\sin^2\theta\, P_{20} + \frac{1}{2}\left(1+\cos^2\theta\right)P_{22}^c, \\ P_{22}^{s\prime} &= -\cos\theta\sin 2\phi\, P_{22}^c. \end{aligned} \tag{7}$$

Within the principal axis frame, the quadrupole Hamiltonian (Equation (5)) may be written in terms of the fundamental nuclear spin operators as

$$\begin{aligned}\mathcal{H}_Q &= \frac{eQV_{zz}}{4I(2I-1)}\left[3I_z^2 - I^2 + \eta\left(I_x^2 - I_y^2\right)\right] \\ &= \frac{eQV_{zz}}{4I(2I-1)}\left[3I_z^2 - I^2 + \frac{\eta}{2}\left(I_+^2 + I_-^2\right)\right] \end{aligned} \tag{8}$$

and diagonalization of this Hamiltonian for the case of the excited nuclear state ($I = \frac{3}{2}$) of ^{169}Tm yields the doubly-degenerate eigenvalues

$$E\left(\pm\frac{3}{2}\right) = +3P_{20}\sqrt{\left(1+\frac{\eta^2}{3}\right)}, \tag{9}$$

$$E\left(\pm\frac{1}{2}\right) = -3P_{20}\sqrt{\left(1+\frac{\eta^2}{3}\right)}. \tag{10}$$

Hence, we obtain the standard expression for the quadrupole splitting (i.e., the energy splitting between the two Mössbauer transitions)

$$\Delta = 6P_{20}\sqrt{\left(1+\frac{\eta^2}{3}\right)} = \frac{eQV_{zz}}{2}\sqrt{\left(1+\frac{\eta^2}{3}\right)}. \tag{11}$$

Table V. Electric quadrupole energies of the five excited states for $I = 2$ (appropriate to ^{166}Er and ^{170}Yb)

$E(+2)$	$E(+1)$	$E(0)$	$E(-1)$	$E(-2)$
$+6P_{20}$	$-3(1+\eta)P_{20}$	$-6P_{20}\sqrt{\left(1+\frac{\eta^2}{3}\right)}$	$-3(1-\eta)P_{20}$	$+6P_{20}\sqrt{\left(1+\frac{\eta^2}{3}\right)}$

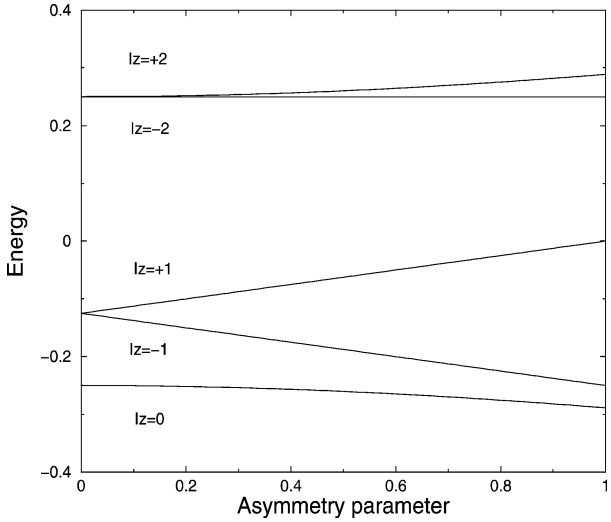

Figure 1. Quadrupole energies of the five $I = 2$ nuclear states in ^{166}Er and ^{170}Yb as functions of the asymmetry parameter η.

In the case of ^{166}Er and ^{170}Yb, the excited nuclear state spin is 2 and the excited state has a multiplicity of 5. The energies of these states, under the action of an EFG, are given in Table V [7]. These eigenvalues and the corresponding eigenvectors were first derived by Sikazono [18] for the case of ^{182}W whose 100.1 keV Mössbauer transition is also $2 \leftrightarrow 0$.

In Figure 1 we show the energies of the five excited nuclear states of ^{166}Er and ^{170}Yb as functions of the asymmetry parameter η. For $\eta = 0$ one obtains three lines whereas for nonzero η there are five lines. This is an important distinction because quadrupole patterns of ^{166}Er and ^{170}Yb are asymmetric and it is therefore possible to determine both the asymmetry parameter η and the quadrupole splitting *including* its sign. This is in contrast to the case of ^{169}Tm where one can only determine the magnitude of the product

$$\frac{eQV_{zz}}{2}\sqrt{\left(1+\frac{\eta^2}{3}\right)}.$$

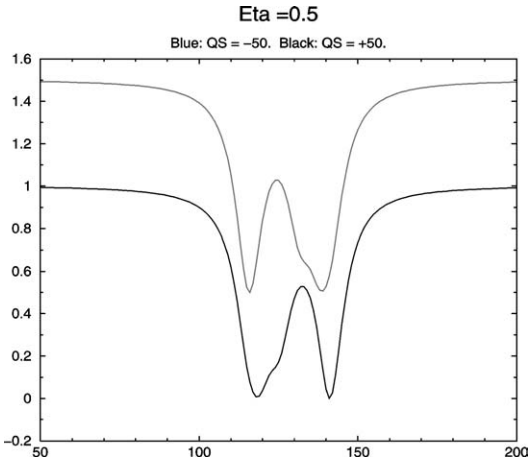

Figure 2. Effect of the sign of the quadrupole splitting parameter (bottom = positive and top = negative) on the quadrupole spectra of ^{166}Er and ^{170}Yb for $\eta = 0.5$.

In Figure 2 we show simulated spectra of ^{166}Er and ^{170}Yb for $\eta = 0.5$. The asymmetry is clear and permits the immediate determination of the sign of the quadrupole splitting.

6. Magnetic dipole interaction

The hyperfine magnetic field at a rare-earth nucleus can be written as

$$B_{\mathrm{hf}} = B_{4\mathrm{f}} + B_{\mathrm{cp}} + B_{\mathrm{p}} + B_{\mathrm{nn}}^{\mathrm{R}} + B_{\mathrm{nn}}^{\mathrm{non}\text{-}R} + B_{\mathrm{ext}}, \tag{12}$$

where the individual terms are

- $B_{4\mathrm{f}}$ is the field due to the incomplete 4f electron shell. The dominant contribution is from the 4f orbital angular momentum L with a weaker dipolar contribution from the 4f spin angular momentum S. These momenta may be projected onto the total momentum to express the field in terms of $\langle J_Z \rangle$ or $\langle J_z \rangle$.
- B_{cp} is the core polarization field which arises from the deformations of the inner shells by the 4f shell. This field is written in the form
$$B_{\mathrm{cp}} = -B_{\mathrm{cp}}^{\mathrm{o}}(g_J - 1)\langle J_Z \rangle, \tag{13}$$
where $B_{\mathrm{cp}}^{\mathrm{o}} \sim$ 6–10 T [3, 6, 8, 19] and g_J is the Landé g-factor of the R^{3+} ion ($g_J = 1.2$ for Er^{3+}).
- B_{p} is the contribution from conduction electron polarization by the spin of the parent R^{3+} ion.
$$B_{\mathrm{p}} = K_{\mathrm{p}}\langle S_Z \rangle = K_{\mathrm{p}}(g_J - 1)\langle J_Z \rangle, \tag{14}$$
where K_{p} is a constant.
- $B_{\mathrm{nn}}^{\mathrm{R}}$ and $B_{\mathrm{nn}}^{\mathrm{non\text{-}R}}$ are transferred hyperfine fields from any surrounding magnetic R and non-R sublattices, respectively, mediated by conduction electron polarization.

- B_{ext} represents any externally applied magnetic fields.

The 'free-ion' field values given in Table I are the sum of $B_{4\text{f}}$ and B_{cp} for the *fully-stretched* electronic state $|\langle J_z\rangle| = J$ and are usually derived from NMR or similar measurements on non-metallic salts where the effects of conduction electrons are absent [3, 4].

Therefore, a measurement of the hyperfine field at the R nucleus in an intermetallic compound, for example, can be deconvoluted to give a *direct* measure of the R^{3+} magnetic moment since all hyperfine field contributions except $B_{\text{nn}}^{\text{non-R}}$ and B_{ext} can be expressed in terms of $|\langle J_z\rangle|$, providing direct proportionality with the R^{3+} magnetic moment. This is an extremely important advantage Mössbauer spectroscopy has over other techniques such as neutron diffraction and magnetometry, as we will show in the following paper [2].

The magnetic hyperfine Hamiltonian can therefore be written as

$$\mathcal{H}_{\text{M}} = -\mu_{\text{n}} \cdot \mathbf{B}_{\text{hf}} = g_{\text{n}}\mu_{\text{N}}\mathbf{I} \cdot \mathbf{B}_{\text{hf}}. \tag{15}$$

7. Mixed magnetic dipole and electric quadrupole interactions

In a real material the direction of magnetic order of the R^{3+} moment, which we can call Z, need not coincide with the principal Z' axis of the EFG and it is necessary to transform one of the axis frames to coincide with the other if we are to obtain the eigenfunctions of the various nuclear states. Clearly, the eigenvalues (i.e., the energy) cannot depend on the final choice of axes.

Therefore, in a coordinate system coincident with the principal axis frame of the EFG the total hyperfine Hamiltonian, i.e., magnetic + quadrupole may be written

$$\begin{aligned}\mathcal{H}_{\text{total}} &= \mathcal{H}_{\text{M}} + \mathcal{H}_{Q} \\ &= g_{\text{n}}\mu_{\text{N}}B_{\text{hf}}\big(I_z\cos\theta + [I_x\cos\phi + I_y\sin\phi]\sin\theta\big) \\ &\quad + \frac{eQV_{zz}}{4I(2I-1)}\big[3I_z^2 - I^2 + \eta\big(I_x^2 - I_y^2\big)\big],\end{aligned} \tag{16}$$

where θ and ϕ are the polar angles of the R^{3+} magnetic moment (and hence the hyperfine field) relative to the EFG principal axis system. We remark here that the total hyperfine field is not necessarily collinear with the R^{3+} magnetic moment due to the possible influence of transferred and/or external fields although any deviation from collinearity will be small. This is the approach used by Kündig [20] in his classic paper. Alternatively, we may take the Z axis to be along the direction of the R^{3+} magnetic moment (hyperfine field) and rotate the quadrupole part of the Hamiltonian onto the magnetic frame. This is appropriate to magnetic rare-earth intermetallics where the magnetic term generally dominates the electric quadrupole.

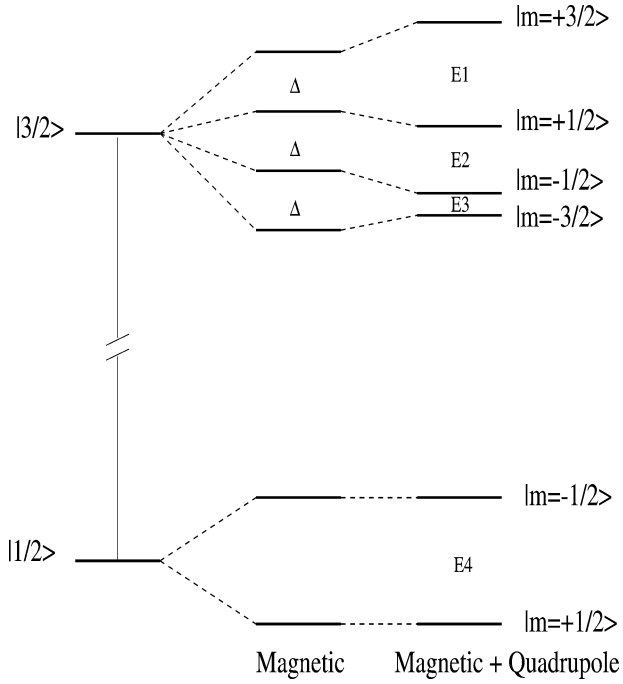

Figure 3. Energy level splittings in ^{169}Tm.

In the simple case where the nuclear hyperfine Hamiltonian is diagonal and $\eta = 0$ and $\theta = 0$, the eigenvalues are given by

$$E_m = -g_{\mathrm{n}}\mu_{\mathrm{N}}B_{\mathrm{hf}}m + \frac{eQV_{zz}}{4I(2I-1)}\left[3m^2 - I(I+1)\right] \tag{17}$$

and it is easy to show that in the case of ^{169}Tm ($\frac{3}{2} \leftrightarrow \frac{1}{2}$) the quadrupole parameter is given by

$$eQV_{zz} = 12P_{20} = (V_6 - V_5) - (V_2 - V_1), \tag{18}$$

whereas for ^{166}Er and ^{170}Yb ($2 \leftrightarrow 0$) we have

$$eQV_{zz} = 24P_{20} = \frac{4}{3}\left[(V_5 - V_4) - (V_2 - V_1)\right], \tag{19}$$

where the line positions V_i are measured in mm/s, numbered from lowest velocity to highest as shown in Figures 3 and 5.

Similarly, in this simple diagonal case the magnetic hyperfine field is given by

$$B_{\mathrm{hf}}^{\mathrm{Tm}}(T) = 0.60(1) \times (V_6 - V_1)\ \mathrm{mm/s}, \tag{20}$$

$$B_{\mathrm{hf}}^{\mathrm{Er}}(T) = 6.77(12) \times (V_5 - V_1)\ \mathrm{mm/s}, \tag{21}$$

$$B_{\mathrm{hf}}^{\mathrm{Yb}}(T) = 6.66(8) \times (V_5 - V_1)\ \mathrm{mm/s}. \tag{22}$$

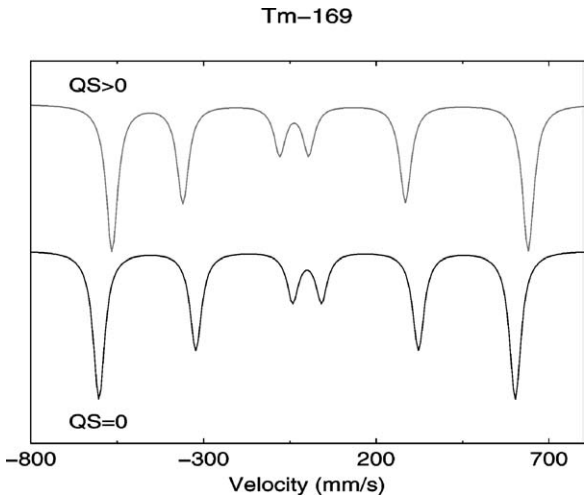

Figure 4. Simulated spectra of ^{169}Tm.

In Figure 3 we show the nuclear energy level scheme for ^{169}Tm due to magnetic dipole and electric quadrupole effects and in Figure 4 we show simulated ^{169}Tm spectra for the simple diagonal magnetic + quadrupole Hamiltonian. It is clear from the asymmetry in the spectra that it is easy to determine the sign of the quadrupole splitting, relative to the hyperfine field. In particular, one need only note the relative sizes of the splittings $V_2 - V_1$ and $V_6 - V_5$.

In Figure 5 we show the nuclear energy level scheme for ^{166}Er due to magnetic dipole and electric quadrupole effects and in Figure 6 we show simulated ^{166}Er spectra for the simple diagonal magnetic + quadrupole Hamiltonian. Once again, it is possible to determine the sign of the quadrupole splitting relative to the field by considering the relative sizes of the line splittings $V_2 - V_1$ and $V_5 - V_4$, although it is not as clear as in the case of ^{169}Tm.

In both simulations, the spectrum with $eQV_{zz} < 0$ is the mirror image of the spectrum with $eQV_{zz} > 0$, reflected through the zero velocity (since we are ignoring isomer shifts in this paper).

In more complex cases one must diagonalise the full hyperfine Hamiltonian and the reader is referred to the articles by Kündig [20], Parker [21] and Matthias *et al.* [22] for tabulations and graphical presentations of the eigenvalues for various nuclear spins.

One method for estimating the nuclear energy levels under the action of the full magnetic + electric quadrupole Hamiltonian is to use second-order perturbation theory. Thus,

$$\begin{aligned} \mathcal{H}_{\text{total}} &= \mathcal{H}_{\text{M}} + \mathcal{H}_{\text{Q}} \\ &= aI_z + P_{20}O_{20} + P_{21}^c O_{21}^c + P_{21}^s O_{21}^s + P_{22}^c O_{22}^c + P_{22}^s O_{22}^s \\ &= \mathcal{H}_0 + \mathcal{H}_1, \end{aligned} \tag{23}$$

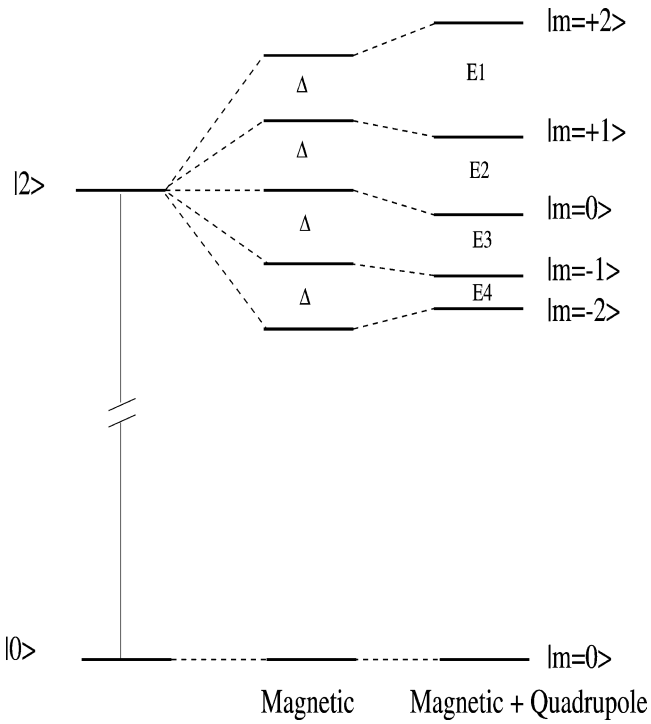

Figure 5. Energy level splittings in ^{166}Er.

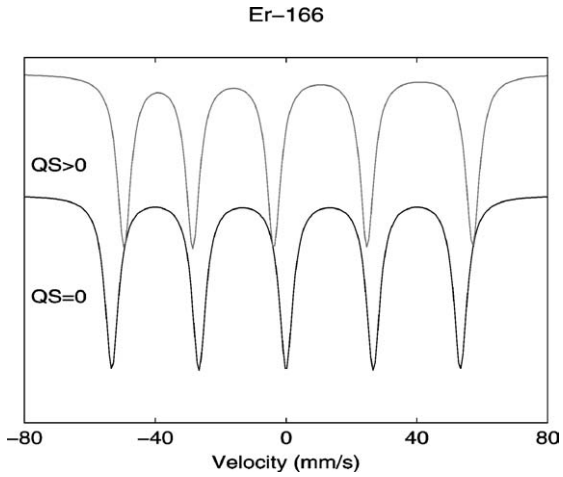

Figure 6. Simulated spectra of ^{166}Er with $B_{\mathrm{hf}} = 700$ T and $eQV_{zz} = +15$ mm/s.

where $\mathcal{H}_0$ is the diagonal part and $\mathcal{H}_1$ is the off-diagonal part of the total Hamiltonian. Using second-order perturbation theory the energies of the various nuclear states are given by

$$E_m = E_m^0 + \sum_n \frac{|\langle m|\mathcal{H}_1|n\rangle|^2}{E_m^0 - E_n^0}. \tag{24}$$

This method was applied to the case of ^{57}Fe by Arif *et al.* [16] and their expressions are also applicable to ^{169}Tm since both transitions are $\frac{3}{2} \leftrightarrow \frac{1}{2}$. In this present paper, we extend the perturbation approach to the case of $2 \leftrightarrow 0$ transitions, relevant to both ^{166}Er and ^{170}Yb. The perturbed energy levels are given by

$$E_m = -m\Delta + P_{20}\big[3m^2 - I(I+1)\big] + \frac{Q_{21}}{16}F_{21} + \frac{Q_{22}}{4}F_{22} \tag{25}$$

where

$$Q_{21} = \big(P_{21}^c\big)^2 + \big(P_{21}^s\big)^2, \tag{26}$$

$$Q_{22} = \big(P_{22}^c\big)^2 + \big(P_{22}^s\big)^2, \tag{27}$$

$$\begin{aligned} F_{21} = {} & \frac{(2m+1)^2[I(I+1) - m(m+1)]}{\Delta - 3P_{20}(2m+1)} \\ & - \frac{(2m-1)^2[I(I+1) - m(m-1)]}{\Delta - 3P_{20}(2m-1)} \end{aligned} \tag{28}$$

and

$$\begin{aligned} F_{22} = {} & \frac{[I(I+1) - m(m+1)][I(I+1) - (m+1)(m+2)]}{2\Delta - 12P_{20}(m+1)} \\ & - \frac{[I(I+1) - m(m-1)][I(I+1) - (m-1)(m-2)]}{2\Delta - 12P_{20}(m-1)}. \end{aligned} \tag{29}$$

In Table VI we give expressions for the energies of the four excited nuclear states in ^{169}Tm, deduced from second-order perturbation theory and in Table VII we give the corresponding expressions for ^{166}Er and ^{170}Yb.

In Tables VI and VII, Δ is the *magnetic-only* splitting between adjacent excited state levels, as shown in Figures 4 and 5.

Fitting of Mössbauer spectra, under the combined action of magnetic dipole and electric quadrupole effects generally involves diagonalising the full Hamiltonian to obtain the energy levels (= eigenvalues) and the transition intensities (from the eigenvectors). Some programs, however, carry out a phenomenological fitting in terms of the experimentally measured line splittings (labelled $E1$–$E4$ in Figures 4 and 5). The individual line positions V_i can be obtained as follows:

$$\begin{bmatrix} V_1 \\ V_2 \\ V_3 \\ V_4 \\ V_5 \end{bmatrix} = \begin{pmatrix} -1 & -2 & -3 & -4 \\ -1 & -2 & -3 & 1 \\ -1 & -2 & 2 & 1 \\ -1 & 3 & 2 & 1 \\ 4 & 3 & 2 & 1 \end{pmatrix} \begin{bmatrix} E1 \\ E2 \\ E3 \\ E4 \end{bmatrix} \times \frac{1}{5}$$

Table VI. Excited state energies for ^{169}Tm ($X1 = (3/4)Q_{21}$ and $X2 = (3/2)Q_{22}$

$E\left(-\frac{3}{2}\right) = \frac{3}{2}\Delta + 3P_{20} + \frac{X1}{\Delta + 6P_{20}} + \frac{X2}{\Delta + 3P_{20}}$
$E\left(-\frac{1}{2}\right) = \frac{1}{2}\Delta - 3P_{20} - \frac{X1}{\Delta + 6P_{20}} + \frac{X2}{\Delta - 3P_{20}}$
$E\left(+\frac{1}{2}\right) = -\frac{1}{2}\Delta - 3P_{20} + \frac{X1}{\Delta - 6P_{20}} - \frac{X2}{\Delta + 3P_{20}}$
$E\left(+\frac{3}{2}\right) = -\frac{3}{2}\Delta + 3P_{20} - \frac{X1}{\Delta - 6P_{20}} - \frac{X2}{\Delta - 3P_{20}}$

Table VII. Excited state energies for ^{166}Er and ^{170}Yb

$E(+2) = -2\Delta + 6P_{20} - Q_{21}\frac{36}{\Delta - 9P_{20}} - Q_{22}\frac{12}{\Delta - 6P_{20}}$
$E(+1) = -\Delta - 3P_{20} - Q_{21}\left(\frac{6}{\Delta - 3P_{20}} + \frac{36}{\Delta - 9P_{20}}\right) - Q_{22}\frac{18}{\Delta}$
$E(0) = -6P_{20} - Q_{21}\left(\frac{6}{\Delta + 3P_{20}} + \frac{6}{\Delta - 3P_{20}}\right) - Q_{22}\left(\frac{12}{\Delta + 6P_{20}} + \frac{12}{\Delta - 6P_{20}}\right)$
$E(-1) = \Delta - 3P_{20} - Q_{21}\left(\frac{36}{\Delta + 9P_{20}} + \frac{6}{\Delta + 3P_{20}}\right) + Q_{22}\frac{18}{\Delta}$
$E(-2) = 2\Delta + 6P_{20} + Q_{21}\frac{36}{\Delta + 9P_{20}} + Q_{22}\frac{12}{\Delta + 6P_{20}}$

for ^{166}Er and ^{170}Yb, and

$$\begin{bmatrix} V_1 \\ V_2 \\ V_3 \\ V_4 \\ V_5 \\ V_6 \end{bmatrix} = \begin{pmatrix} -3 & -6 & -9 & -6 \\ -3 & -6 & 3 & -6 \\ -3 & 6 & 3 & -6 \\ -3 & -6 & 3 & 6 \\ -3 & 6 & 3 & 6 \\ 9 & 6 & 3 & 6 \end{pmatrix} \begin{bmatrix} E1 \\ E2 \\ E3 \\ E4 \end{bmatrix} \times \frac{1}{12}$$

for ^{169}Tm.

An important point arising from the second-order perturbation method is that it allows one to derive inequalities which can be used to determine if a proposed 'fit' to a spectrum is physical or otherwise. The factors Q_{21} and Q_{22} are positive, since they depend on the squares of the relevant quadrupole parameters, so one

can show that in the case of ^{169}Tm, for example, the line splittings must obey the inequalities [16]

$$E1 + E3 \geqslant 2\Delta, \tag{30}$$

$$E1 + E2 + E3 \geqslant 3\Delta. \tag{31}$$

8. Conclusion

The *local* nature of rare-earth Mössbauer spectroscopy makes it ideally suited to the determination of rare-earth ionic magnetic moments and valences in metallic and non-metallic compounds. In this paper, we have presented a summary of the Mössbauer effect in ^{166}Er, ^{169}Tm and ^{170}Yb.

Acknowledgements

J.M.C. is grateful for the hospitality of the Centre for the Physics of Materials, Department of Physics, McGill University, Montreal, Canada, where some of this work was carried out during a sabbatical visit. This work was supported by grants from the Australian Research Council, the Australian Nuclear Science and Technology Organisation, the Australian Academy of Science, the Natural Sciences and Engineering Research Council of Canada and Fonds pour la formation de chercheurs et l'aide à la recherche, Québec.

References

1. Stevens, J. G. *et al.*, Information booklet, Mössbauer Effect Data Centre.
2. Ryan, D. H. and Cadogan, J. M., *Hyp. Interact.*, to be published.
3. Bleaney, B., In: R. J. Elliott (ed.), *Magnetic Properties of Rare Earth Metals*, Plenum, London, 1979, Chapter 8.
4. Bleaney, B., In: K. A. Gschneidner Jr and L. Eyring (eds), *Handbook on the Physics and Chemistry of Rare Earths*, Vol. 11, Elsevier Science, Amsterdam, 1988, Chapter 77.
5. Abragam, A., *The Principles of Nuclear Magnetism*, Clarendon Press, Oxford, 1961.
6. Guimarães, A. P., *Magnetism and Magnetic Resonance in Solids*, Wiley-Interscience, New York, 1998, pp. 173–174.
7. Dunlap, B. D., In: J. G. Stevens and V. E. Stevens (eds), *Mössbauer Effect Data Index*, Plenum, New York, 1970, pp. 25–40.
8. McCausland, M. A. H. and Mackenzie, I. S., *Adv. in Phys.* **28** (1979), 305–456.
9. Hodges, J. A., Jehanno, G., Schuhl, A. and Berthier, Y., *Hyp. Interact.* **11** (1981), 29–35.
10. Berthier, Y. and Devine, R. A. B., *J. Appl. Phys.* **52** (1981), 2071–2073.
11. Baker, J. M. and Williams, F. I. B., *Proc. Roy. Soc. A* **267** (1962), 283–294.
12. Berthier, Y., Devine, R. A. B. and Butera, R. A., In: E. N. Kaufmann and G. K. Shenoy (eds), *Nuclear and Electron Resonance Spectroscopies Applied to Materials Science, Proc. Annual MRS Meeting*, Boston, 1980, p. 449.
13. Bleaney, B., Bowden, G. J., Cadogan, J. M., Day, R. K. and Dunlop, J. B., *J. Phys. F Metal. Phys.* **12** (1982), 795–811.
14. Bonville, P., Gonzalez-Jimenez, F., Imbert, P. and Varret, F., *J. Phys. C* **6** (1974), 575–579.

15. Coehoorn, R., Buschow, K. H. J., Dirken, M. W. and Thiel, R. C., *Phys. Rev. B* **42** (1990), 4645–4655.
16. Arif, S. K., Bunbury, D. St. P., Bowden, G. J. and Day, R. K., *J. Phys. F Metal. Phys.* **5** (1975), 1037–1047.
17. Rudowicz, C., *J. Phys. C Solid State Phys.* **18** (1985), 1415–1430.
18. Sikazono, N., Takekoshi, H. and Shoji, T., *J. Phys. Soc. Japan* **20** (1965), 271–275.
19. Netz, G., *Z. Phys. B* **63** (1986), 343–349.
20. Kündig, W., *Nucl. Instrum. Methods* **48** (1967), 219–228.
21. Parker, P. M., *J. Chem. Phys.* **24** (1956), 1096–1102.
22. Matthias, E., Schneidner, W. and Steffen, R. M., *Phys. Rev.* **125** (1962), 261–268.